International Journal of Naval Architecture and Ocean Engineering 12 (2020) 376–386

Contents lists available at ScienceDirect

International Journal of Naval Architecture and Ocean Engineering

journal homepage: http://www.journals.elsevier.com/international-journal-of-naval-architecture-and-ocean-engineering/

Vector form intrinsic finite-element analysis of static and dynamic behavior of deep-sea flexible pipe

Han Wu [a, b], Xiaohui Zeng [a, b, *], Jianyu Xiao [c], Yang Yu [d], Xin Dai [d], Jianxing Yu [d]

[a] Key Laboratory for Mechanics in Fluid Solid Coupling Systems, Institute of Mechanics, Chinese Academy of Sciences, Beijing, 100190, China
[b] School of Engineering Science, University of Chinese Academy of Sciences, Beijing, 100049, China
[c] Institute of Deep Sea Science and Engineering, Chinese Academy of Sciences, Sanya, 572000, Hainan, China
[d] State Key Laboratory of Hydraulic Engineering Simulation and Safety, Tianjin University, Tianjin, 300350, China

ARTICLE INFO

Article history:
Received 20 July 2019
Received in revised form
20 March 2020
Accepted 15 April 2020
Available online 11 May 2020

Keywords:
Vector form intrinsic finite-element
Flexible pipe
3D beam element
Spatial configuration
Dynamic behavior

ABSTRACT

The aim of this study was to develop a new efficient strategy that uses the Vector form Intrinsic Finite-element (VFIFE) method to conduct the static and dynamic analyses of marine pipes. Nonlinear problems, such as large displacement, small strain, and contact and collision, can be analyzed using a unified calculation process in the VFIFE method according to the fundamental theories of point value description, path element, and reverse motion. This method enables analysis without the need to integrate the stiffness matrix of the structure, because only motion equations of particles established according to Newton's second law are required. These characteristics of the VFIFE facilitate the modeling and computation efficiencies in analyzing the nonlinear dynamic problem of flexible pipe with large deflections. In this study, a three-dimensional (3-D) dynamical model based on 3-D beam element was established according to the VFIFE method. The deep-sea flexible pipe was described by a set of spatial mass particles linked by 3-D beam element. The motion and configuration of the pipe are determined by these spatial particles. Based on this model, a simulation procedure to predict the 3-D dynamical behavior of flexible pipe was developed and verified. It was found that the spatial configuration and static internal force of the mining pipe can be obtained by calculating the stationary state of pipe motion. Using this simulation procedure, an analysis was conducted on the static and dynamic behaviors of the flexible mining pipe based on a 1000-m sea trial system. The results of the analysis proved that the VFIFE method can be efficiently applied to the static and dynamic analyses of marine pipes.

1. Introduction

Flexible mining pipe is one of the key components in deep-sea mining systems. The traction of nodule collector, movement of the buffer, and hydrodynamic force causes very large oscillation amplitude, which results in a typical small strain and large displacement problem. Therefore, the coupling process of flexible mining pipe is different from rigid mining pipe and requires special analysis of the nonlinear dynamic characteristics.

Patel and Seyed (1995) reviewed existing methods and analysis techniques of flexible risers. Three methods can be applied for the static and dynamic analyses of flexible pipes: lump mass method, finite difference method, and finite-element method. Ghadimi (1988) analyzed the dynamics of flexible risers in three-dimensional space using lumped mass discretization method. Raman-Nair and Baddour (2003) formulated equations describing the 3D motion of a marine riser according to lumped masses method using Kane's formalism. Brown et al. (1989); Burgess (1991); and Jain (1994) analyzed the static and dynamic response of flexible marine pipe using finite difference technique. Sakamoto and Hobbs (1995) proposed a computational technique for the static and dynamic analyses of flexible pipes using the dynamic relaxation method with a finite difference discretization. Chatjigeorgiou (2008, 2010) proposed a finite difference numerical scheme to study the dynamic problems of 2D and 3D fluid-conveying catenary risers. Garrett (1982) proposed a three-

* Corresponding author. Key Laboratory for Mechanics in Fluid Solid Coupling Systems, Institute of Mechanics, Chinese Academy of Sciences, Beijing, 100190, China.
E-mail addresses: wuhan@imech.ac.cn (H. Wu), zxh@imech.ac.cn (X. Zeng), xiaojy@idsse.ac.cn (J. Xiao), yang.yu@tju.edu.cn (Y. Yu), 18802280176@139.com (X. Dai), yjx2000@tju.edu.cn (J. Yu).
Peer review under responsibility of Society of Naval Architects of Korea.

https://doi.org/10.1016/j.ijnaoe.2020.04.003

Nomenclature

L	pipe length
H	height of the buffer from the seabed
E	young's modulus
G	shear modulus
D_O	outer diameter
D_I	inner diameter
W_{ra}	weight in air
W_{rw}	weight in water
ρ_f	seawater density
ρ_I	inflow density
$\boldsymbol{x}_a$	position vector of node a
$\boldsymbol{\theta}_a$	angle vector of node a
$\boldsymbol{M}_a$	mass matrix of node a
$\boldsymbol{I}_a$	rotational inertia matrix of node a
μ	damping parameter
$\boldsymbol{P}_a(t)$	external force vector
$\boldsymbol{Q}_a(t)$	external moment vector
$\boldsymbol{f}_a(t)$	internal force vector
$\boldsymbol{m}_a(t)$	internal moment vector
$\boldsymbol{e}^n$	principal axis vector
$\boldsymbol{R}_\beta$	transformation matrix
$\boldsymbol{\beta}$	rotation vector of element
$\boldsymbol{p}$	uniform load on element
$\boldsymbol{p}_{mass}$	gravity per unit length of element
$\boldsymbol{p}_{buoyancy}$	buoyancy of every unit length of element
$\boldsymbol{p}_{cross\text{-}flow}$	transverse flow damping force per unit length of element
$\boldsymbol{p}_{tangentail}$	tangential damping force per unit length of element
C_d	cross-flow drag force coefficient
$C_{d,l}$	tangential damping force coefficient

dimensional finite-element model of an inextensible elastic rod with equal principal stiffness. Webster et al. (2012) extended Garrett's theory to include the possibility of large stretch. Owen and Qin (1986) calculated the deformation and strain of flexible pipe based on finite-element method (FEM). McNamara and Hibbit (1986) as well as McNamara et al. (1988) used FEM to simulate the motions and forces on a flexible riser. Park and Jung (2002) used FEM to numerically analyze lateral responses of a long slender marine structure under combined parametric and forcing excitation in time domain.

Flexible deep-sea mining conveying pipe is very long and moves under various loads, which leads to dramatical deflections. Thus, it suffers from the geometric nonlinear problem of small strain and large displacement. Using traditional FEM to solve the large displacement problem of the mining pipe can be achieved by including high-order term in the strain calculations and taking into consideration the influence of deformation when deriving the equilibrium equation. In addition, it is difficult to distinguish the pure deformation of element from the rigid body motion. Therefore, using FEM here requires special techniques. Moreover, these slender pipes might experience various complicated nonlinear contacts, such as seabed contact, and nonlinear changes in the material under working conditions. In the computation process, traditional FEM relies on the assembled stiffness matrix. It requires complicated matrix operations when dealing with nonlinear problems. Because of its complicated theory and low computational efficiency, it is difficult to implement traditional FEM in the dynamic analysis of flexible mining pipe under complex loads and constraints (Lu and Yao, 2012). Shih et al. (2004) have pointed out that using traditional FEM to calculate the internal force of a structure with a much larger rigid body displacement compared to its pure deformation may lead to instability of the calculation process.

The Vector form Intrinsic Finite-element (VFIFE) method was proposed by Shih et al. (2004) and Ting et al. (2012, 2004a, 2004b). This method discretizes the structure into a series of nodes linked by elements, in which the structure mass is concentrated at the nodes and the elements are weightless. To solve the internal force of the element, the rigid body displacement and the pure deformation are separated by introducing reversed movement. Then, the unbalanced resultant force on the node is used to calculate the motion of the node according to Newton's second law of motion. This enables the behavior of the system to be described through tracing the nodes' motion. The motion process is divided into a series of path elements. In a path element, the strain of the element is small, but the displacement might be large and the node motion is continuous. Between two path elements, the motion of the nodes may be discontinuous, while the structural combinations; node forces; and element characteristics may vary. The processing and solution using the VFIFE approach do not require the establishment of stiffness matrix, and hence when the structure has a large displacement, the solution does not fail because of an ill-conditioned matrix. The VFIFE method assumes that every node satisfies Newton's law of motion, and it belongs to a strong form; while the traditional FEM considers the overall energy balance in order to establish equations, and it belongs to a weak form. Therefore, no matrix solving is required for the VFIFE method, which enables it to change the correlation between nodes at any time. In addition, a unified main analysis procedure can be used for the simulation of problems with complex discontinuous behaviors such as collision and contact. Table 1 summarizes the difference between the traditional FEM and the VFIFE method. These characteristics of VFIFE enhance the computation efficiency and facilitate the modeling of flexible pipes that involve nonlinearities such as constraint, geometric, and material nonlinearities.

Many scholars have used the VFIFE method to carry out a variety

Table 1
Difference between the traditional FEM and the VFIFE method.

	traditional FEM	VFIFE method
Result of discretization	elements	particles
Computational process	Special treatment for discontinuities. It is difficult to increase or decrease the element and change boundary conditions in the computational process	Using path element to increase and decrease elements and change boundary conditions in the computational process
Pure deformation	Eliminating rigid body displacement by derivation	Distinguishing rigid body displacement and pure deformation by inverse motion
Stiffness matrix	Yes	No
Basic theory	Variational principle	Newton's second law of motion

of dynamic behavior analysis of engineering structures. Wu et al. (2007) conducted a motion analysis of 3D membrane structures. Wu (2013) used the VFIFE method to analyze the contact collision problem with global large displacement, large deflection, and nonlinear material properties. Xu and Lin (2017) developed a fast VFIFE mechanical analysis model for long-distance pipelines. Duan et al. (2014) studied the whole vibration and collapse process of cable-stayed bridges under earthquakes by using plane beam element in the VFIFE method. Duan et al. (2019) used VFIFE to analyze the bridge systems of the trains taking into consideration the coach-coupler effect. Hou et al. (2018); Hou and Fang (2018) applied this method to static contact analysis of spiral bevel gear as well as solid structure analysis with large deformation. Thus, VFIFE is a promising method for analyzing the offshore template structures regardless of their dynamic characteristic, large displacement motion, or structural type (Lee et al., 2007). Chang et al. (2010) studied the dynamic behavior of offshore structures under nonlinear wave forces using the planar frame elements in the VFIFE.

VFIFE was also used in the field of ocean pipeline dynamics analysis. Li et al. (2016); Li et al. (2018a,b) used VFIFE for the static and dynamic analyses of TTR and SCR. However, only the plane movement of TTR and SCR, where the boundary conditions are relatively simple, were analyzed. Flexible mining pipe exhibits three-dimensional motion under complex constraints and load conditions; thus, the plane motion analysis cannot be used in this case.

In this study, a three-dimensional nonlinear fluid-solid coupling dynamic model and a dynamic response prediction simulation program based on the VFIFE method were established to be used with a deep-sea mining pipe. The analysis of static and dynamic characteristics of flexible mining pipes was conducted based on the self-developed program. The equilibrium configuration and the force of the pipe on the nodule collector were analyzed in different collector positions and different buoyancy material arrangements. The deformation and dynamic response of mining pipes were simulated during the movement of nodule collector and buffer. The analysis verified the reliability of the VFIFE method and the self-developed program. Therefore, this study delivered an efficient and reliable mathematical model and numerical simulation method for the static and dynamic analyses of mining pipes as well as other deep-sea slender rods. In addition, the results of the numerical simulation can provide guidance for safety considerations of seabed mining.

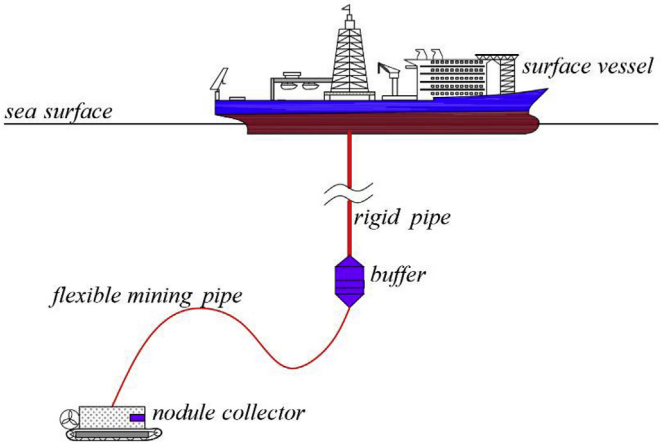

Fig. 1. The 1000-m seabed mining system in China.

2. Flexible mining pipe

Fig. 1 shows a classical deep-sea trial mining system of 1000 m that was designed in 2001 by China Ocean Mineral Resources R & D Association. The mining system is mainly composed of mining vessels, rigid mining lifting pipes, buffers, nodule collectors, and flexible mining pipes. The traction of the nodule collector, movement of the buffer, and hydrodynamic force will cause very large oscillation amplitude, which results in a typical small strain and large displacement problem. Here the flexible mining pipe was analyzed using static and dynamic analyses based on the VFIFE method. Table 2 provides the design parameters of the flexible mining pipe. The pipe was assumed to have hinged ends. In addition, only the pipe half near the nodule collector was assumed to be made of buoyancy materials and the buoyancy was assumed to be twice the wet weight of the pipe.

3. Vector form intrinsic finite-element method

3.1. Governing equations

According to the basic principle of the VFIFE method, the flexible mining pipe was discretized into a series of mass nodes linked by 3D beam element (Fig. 2). The global coordinate system is XYZ, element coordinate system of any arbitrary element AB is $X_sY_sZ_s$. The motion was decomposed into path elements in time domain. The shape and position of the mining pipe were described by tracing the nodal movements, which are computed according to Newton's Second Law as follows:

$$\begin{aligned} \boldsymbol{M}_a\ddot{\boldsymbol{x}}_a + \mu\boldsymbol{M}_a\dot{\boldsymbol{x}}_a &= \boldsymbol{P}_a(t) + \boldsymbol{f}_a(t), \\ \boldsymbol{I}_a\ddot{\boldsymbol{\theta}}_a + \mu\boldsymbol{I}_a\dot{\boldsymbol{\theta}}_a &= \boldsymbol{Q}_a(t) + \boldsymbol{m}_a(t), \end{aligned} \tag{1}$$

where a is node number, t is time; $\boldsymbol{x}_a$ and $\boldsymbol{\theta}_a$ are the position and angle vector, respectively, of node a in the global coordinate system; $\boldsymbol{M}_a$ and $\boldsymbol{I}_a$ are the mass matrix and the rotational inertia matrix, respectively, of node a; μ is the damping parameter; $\boldsymbol{P}_a(t)$ and $\boldsymbol{Q}_a(t)$ are the external force and moment, respectively; and $\boldsymbol{f}_a(t)$ and $\boldsymbol{m}_a(t)$ are the internal force and moment, respectively.

The above equation is generally time-integrated using the central difference method.

$$\begin{cases} \boldsymbol{x}_{a,n+1} = c_1(\Delta t)^2\boldsymbol{M}_a^{-1}(\boldsymbol{P}_a(t) + \boldsymbol{f}_a(t)) + 2c_1\boldsymbol{x}_{a,n} - c_2\boldsymbol{x}_{a,n-1}, \\ \boldsymbol{\theta}_{a,n+1} = c_1(\Delta t)^2\boldsymbol{I}_a^{-1}(\boldsymbol{Q}_a(t) + \boldsymbol{m}_a(t)) + 2c_1\boldsymbol{\theta}_{a,n} - c_2\boldsymbol{\theta}_{a,n-1}, \end{cases} \tag{2}$$

where $c_1 = 1/(1+\mu\Delta t/2)$, $c_2 = c_1(1-\mu\Delta t/2)$.

Table 2
Design parameters of the flexible mining pipe (Xiao, 2012).

parameter	symbol	value	Unit
Pipe length	L	400	m
Height of the buffer from the seabed	H	100	m
Young's modulus	E	0.4	GPa
Shear modulus	G	0.15	GPa
Outer diameter	D_O	0.205	m
Inner diameter	D_I	0.15	m
Weight in air	W_{ra}	30	kg/m
Weight in water	W_{rw}	18	kg/m
Seawater density	ρ_f	1025	kg/m^3
Internal flow density	ρ_I	1100	kg/m^3

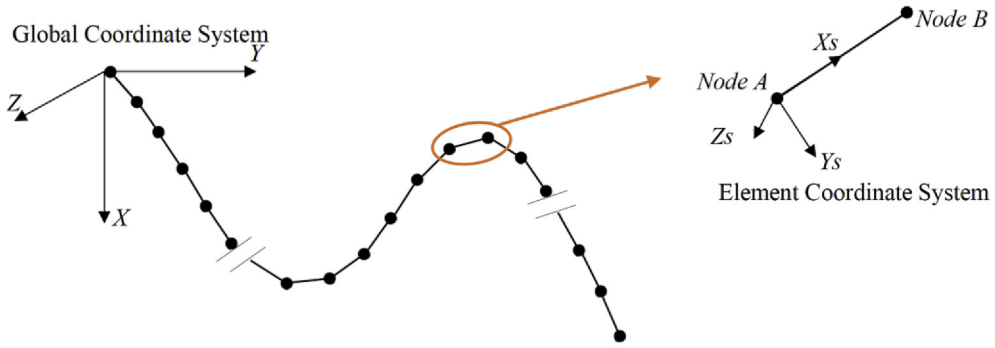

Fig. 2. The VFIFE analysis model of the flexible mining pipe.

3.2. Internal force

The internal force acting on node *a* is the resultant force from its adjacent elements:

$$\boldsymbol{f}_a = \sum_{i=1}^{N} \boldsymbol{f}_a^i \,,\ \boldsymbol{m}_a = \sum_{i=1}^{N} \boldsymbol{m}_a^i, \tag{3}$$

N is the number of elements adjacent to node *a*, $\boldsymbol{f}_a^i$, *and* $\boldsymbol{m}_a^i$ is the internal force and moment, respectively, of the *i*-th element acting on node *a*.

The node displacement in a time step is composed of element deformation and rigid element motion. The rigid element motion has a negligible effect on the element internal forces and moments. Therefore, it can be eliminated using fictitious reversed movement according to the VFIFE method (Fig. 3). Next, the element deformation is obtained, and the element internal forces and moments are calculated.

Fig. 3 shows that element *AB* moves from position A_nB_n to position $A_{n+1}B_{n+1}$ within the path element $t_n \le t \le t_{n+1}$. As the principal axis vector is known to be ($\boldsymbol{e}_{xs}^n$, $\boldsymbol{e}_{ys}^n$, $\boldsymbol{e}_{zs}^n$) at time t_n, the position of element *AB* at t_n and t_{n+1} in the global coordinate system can be calculated by integrating using the central difference method. Thus, the principal axis vector ($\boldsymbol{e}_{xs}^{n+1}$, $\boldsymbol{e}_{ys}^{n+1}$, $\boldsymbol{e}_{zs}^{n+1}$) at t_{n+1} can be calculated. According to the principal axis vectors in t_n and t_{n+1}, the transformation matrix $\boldsymbol{R}_\beta$ and the rotation vector $\boldsymbol{\beta}$ of the element can be obtained. (For more details about fictitious reversed movement and calculating the internal forces of the VFIFE 3D beam element, refer to the study by Ting et al., 2012.)

3.3. External force

External forces include those acting on the node as well as distributed forces applied on the adjacent elements. The derivation of the equivalent nodal force (moment) of the element distribution load is found in the study of Ting et al. (2012).

The distributed forces acting on a flexible pipe under ocean include gravity, buoyancy, and hydrodynamic loads.

(1) Gravity

The gravity of every unit length of element *AB*

$$\boldsymbol{p}_{mass} = \left(\rho A g + \rho_I \pi D_I^2 g \,/\, 4\right)\boldsymbol{e}_x^n. \tag{4}$$

(2) Buoyancy

Buoyancy of every unit length of element *AB*

$$\boldsymbol{p}_{buoyancy} = -\rho_f \left[g\boldsymbol{e}_x^n + \dot{\boldsymbol{v}}_f\right] \cdot \pi D_O^2 \,/\, 4. \tag{5}$$

(3) Hydrodynamic loads

The Morison formula was used to calculate the fluid damping forces acting on the pipe. The transverse hydrodynamic force per unit length of element *AB* is given as follows:where, C_d is the cross-flow drag force coefficient, and $\boldsymbol{v}_{relative}$ is the relative velocity of the

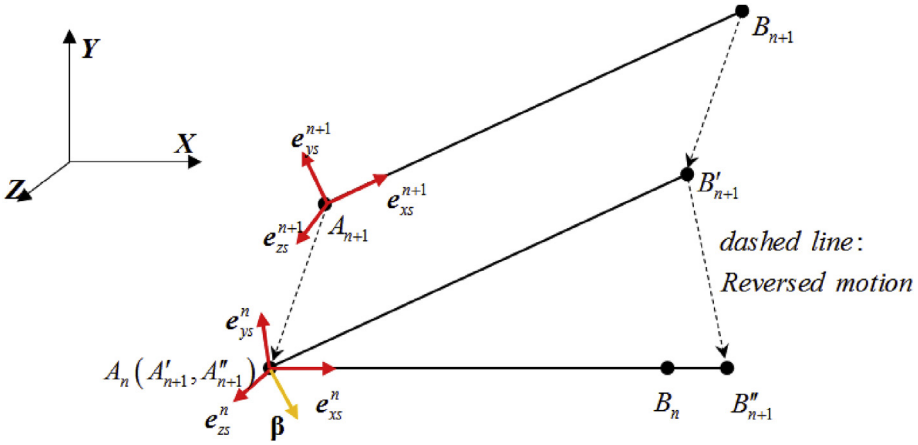

Fig. 3. Fictitious reversed rigid body motion of a 3D beam element.

fluid to the member. $\boldsymbol{N} = \boldsymbol{I} - \boldsymbol{e}^n_{xs}(\boldsymbol{e}^n_{xs})^T$. C_m is the additional mass coefficient.

The tangential hydrodynamic force per unit length of element AB is given as follows:

$$\boldsymbol{p}_{cross-flow} = 0.5C_d\rho_f D_O\left[\boldsymbol{v}_{relative} - (\boldsymbol{v}_{relative}\cdot\boldsymbol{e}^n_{xs})\boldsymbol{e}^n_{xs}\right]\cdot\left|\boldsymbol{v}_{relative} - (\boldsymbol{v}_{relative}\cdot\boldsymbol{e}^n_{xs})\boldsymbol{e}^n_{xs}\right| - 0.5\rho_f A_{out} l_0 C_m(\ddot{\boldsymbol{x}}_A + \ddot{\boldsymbol{x}}_B)\boldsymbol{N}. \tag{6}$$

$$\boldsymbol{p}_{tangentail} = C_{d,l}\frac{\rho_f}{2}\pi D_O\left[(\boldsymbol{v}_{relative}\cdot\boldsymbol{e}^n_{xs})\right]\left|(\boldsymbol{v}_{relative}\cdot\boldsymbol{e}^n_{xs})\right|\boldsymbol{e}^n_{xs} - 0.5\rho_f A_{out} l_0 C_m(\ddot{\boldsymbol{x}}_A + \ddot{\boldsymbol{x}}_B)\cdot\boldsymbol{e}^n_{xs}, \tag{7}$$

where, $C_{d,l}$ is the tangential damping force coefficient.

3.4. Equivalent node mass and rotational inertia

3.4.1. Mass matrix

The translational mass of the pipe distributed on the node includes the mass of the node and the equivalent mass of its connected elements. In the calculations of a homogeneous pipe, when the nodes are evenly distributed, the total mass of the element will be equally distributed to the spatial nodes. In element AB, the mass matrix in the path element $t_n \le t \le t_{n+1}$ can be calculated as follows:

$$\boldsymbol{M}_{AB} = \rho_l A_{in} l_0 \boldsymbol{N} + \rho A l_0 \times diag[111] \tag{8}$$

where ρ is the pipe density, A is the cross-sectional area, l_0 is the element length.

The total mass of elements is evenly distributed to the nodes A and B:

$$\boldsymbol{m}_{fA} = \boldsymbol{m}_{fB} = \boldsymbol{M}_{AB}/2 \tag{9}$$

$\boldsymbol{m}_{fA}$ and $\boldsymbol{m}_{fB}$ can be used to integrate the equivalent translational mass matrix of the nodes A and B.

3.4.2. Rotational inertia matrix

The moments of inertia distributed on a node also include the node concentrated inertia and the equivalent node inertia of the connected element. The moments of inertia in the homogeneous cylinder element AB in the element coordinate system are given as follows:

$$\begin{aligned} I_{Axs} &= I_{Bxs} = \left(\pi d^4_{out} - \pi d^4_{in}\right)\times\rho l_0/64 \\ I_{Ays} &= I_{Bxs} = I_{Azs} = I_{Bxs} = \left(\pi d^4_{out} - \pi d^4_{in}\right)\times\rho l_0/128 \end{aligned} \tag{10}$$

In the global coordinate system, the equivalent inertia matrix can be expressed as follows:

$$\boldsymbol{I}_j = \boldsymbol{\Omega}^T diag\left[I_{jxs} I_{jys} I_{jzs}\right]\boldsymbol{\Omega}\ (j = A, B) \tag{11}$$

The total inertia of nodes A and B in the global coordinate system can be obtained by adding up the inertia of all the elements connected to the node.

4. Program and validation

Fortran was used to develop a three-dimensional dynamic response analysis program for flexible mining pipes based on the VFIFE method. The results of this program were compared to those obtained from commercial software and in the literature to verify the reliability of the program. This program is not limited to the dynamic analysis of flexible mining pipes and can be used for several elongated structures commonly used in marine engineering. This section includes the verification process of the developed program through the analysis of TTR and SCR.

4.1. Dynamic analysis of TTR

The overall motion analysis of TTR conducted by Abaqus was used to verify the VFIFE program developed here. The simulated prototype is a top tensioned production riser connected from the top to the christmas tree, which is connected to the platform by four tensioners. The christmas tree is described by an equivalent point mass. The tensioner is modeled by a nonlinear spring. The riser can be divided into four sections along the pipe length according to the equivalent density. The total length of the riser is 435.8 m. The material densities in all the sections are listed in Table 3. The total number of elements simulated in both cases is 400.

Table 4 contains a comparison between the natural frequencies of the TTR vertical vibrations, in which the uniform density refers to that of a riser equivalent to a vertically uniform slender pipe and equals 8000 kg/m^3. The theoretical value of the TTR's natural frequency in case of uniform density can be estimated as follows: $\omega = [(2j-1)\pi\sqrt{E/\rho}]/2l$. The results in Table 4 indicate that the natural frequency calculated by VFIFE is consistent with those obtained by Abaqus and the theoretical solution.

Fig. 4 shows the dynamic responses of the riser when the platform is heaving. Fig. 4(a) and (b) illustrate comparisons of the tension at the tension ring and the reaction force of the bearing with maximum relative errors of 4.7% and 3.4%, respectively. Fig. 4(c) and (d) show comparisons of the states of motion at the tension ring and the middle point of the riser, respectively, with an error of less than 5%. The results of the VFIFE program are in good agreement with those of the theoretical solution and the Abaqus simulation. In addition, the VFIFE method saved 60% of the computation time for this example compared to Abaqus.

4.2. Static analysis of SCR

The static position and bending moment distribution of the SCR

Table 3
Summary of material densities.

Section name	Length (m)	Material density (kg/m^3)
TJ	17.9	52,842
Spashzone Joint	22	15,145
Standard Joint	381.3	5867
TSJ	14.6	22,809

Table 4
Comparison between the natural frequencies calculated by different tools.

	Theoretical value	Abaqus	Self-developed program	Relative error
uniform density	0.348	0.349	0.351	<1%
variable density		0.414	0.419	<1%

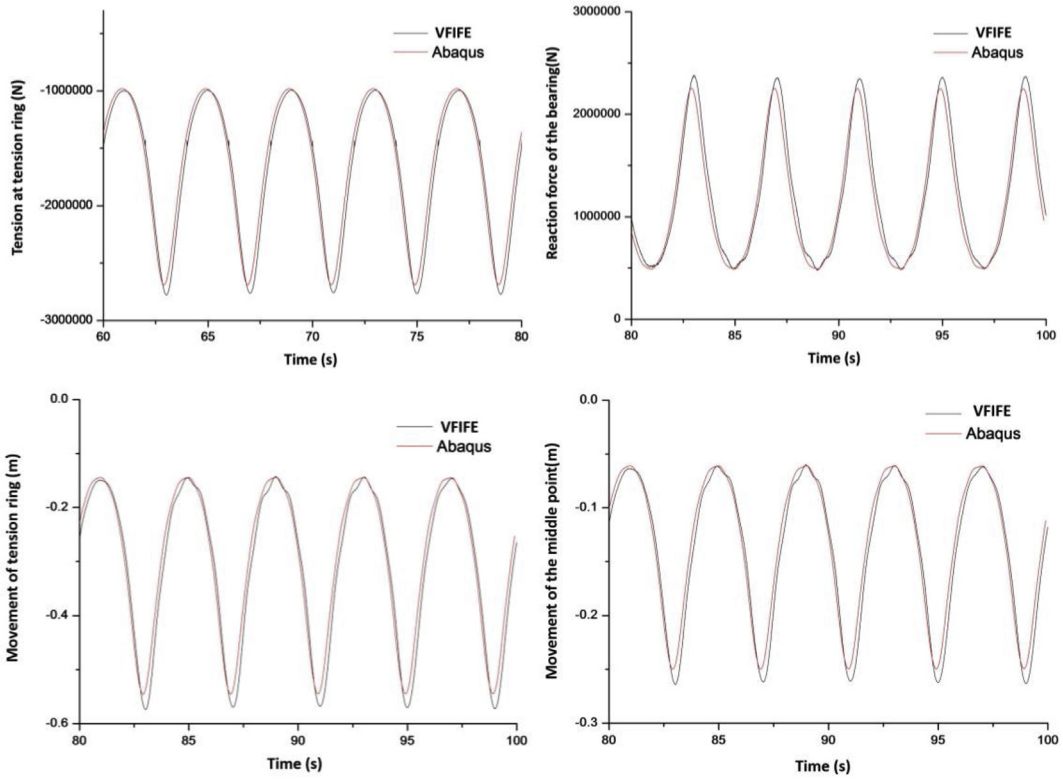

Fig. 4. Comparison between the TTR dynamic responses: (a) Tension at tension ring; (b) Reaction force of the bearing; (c) Movement of tension ring; (d) Movement of the middle point.

were calculated using the VFIFE program and compared to those calculated in the study conducted by Bai et al. (2015). Before performing the static equilibrium analysis based on the VFIFE method, the internal force of the SCR state should be set to zero. This is followed by a dynamic analysis, and the static equilibrium is achieved when the stabilized state is reached.

Bai et al. (2015) compared the analyses results of the commercial software Orcaflex with the results calculated by the software (Cable 3D RSI) developed in their study. Fig. 5 shows the comparison between the static configuration and bending moment of SCR

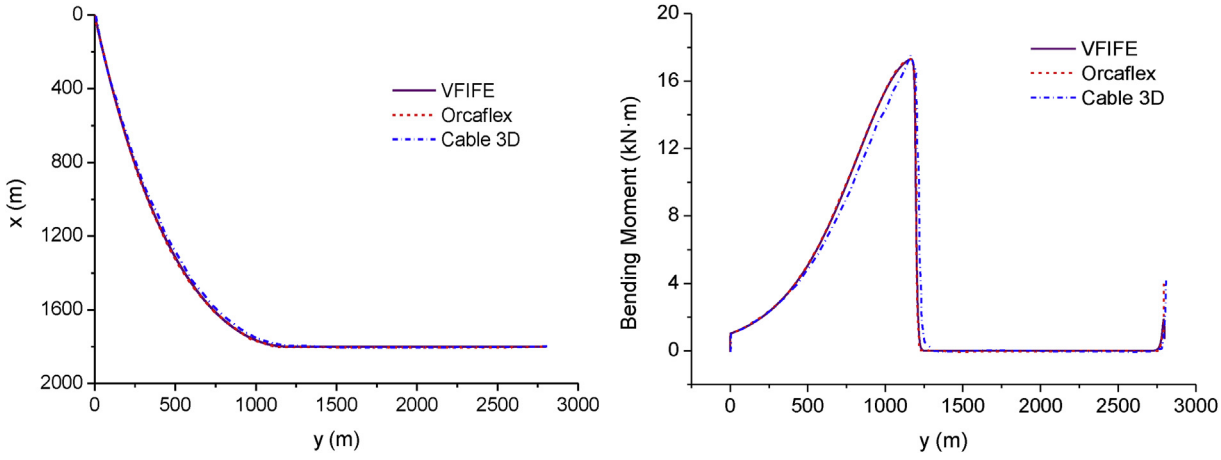

Fig. 5. Comparison between the SCR static configuration and static bending moment estimated by three different analyses.

calculated by the VFIFE and those estimated by Bai's analysis. The comparison shows that the static configuration and bending moment based on the VFIFE method completely coincide with the Orcaflex results and are close to the results of the Cable 3D RSI. This comparative analysis demonstrated the validity and accuracy of the method and program proposed in this study.

5. Results

After validating the VFIFE program, static state and dynamic response analyses of a flexible mining pipe were carried out. In the simulation, the pipe was discretized into 601 mass points, and the initial position of the buffer was set at the origin point of the spatial coordinate system. Fig. 2 shows that the downward direction was set on the positive *x*-axis direction, the nodule collector is in the positive direction of the *y*-axis, and the direction perpendicular on both of them was set in the positive *z*-axis direction. The connections between the pipe and the nodule collector as well as between the pipe and the buffer are simply supported.

5.1. Static state analysis

The detailed analysis process of the flexible mining pipe static state using VFIFE method is as follows: At time zero, the pipe was straight with no bending or stretching.; the initial position of the tail end of the pipe was (100, 387, 0), and the position of the top end of the pipe was (100, −13, 0) considering that the extreme position of the nodule collector was 387.3 m from the buffer in the horizontal direction. During the calculation, the top end of the pipe moves slowly upwards along a parabolic trajectory, and then stops at the coordinate origin (i.e., the buffer). Next, the calculation continues until the motion becomes stationary, and the static equilibrium position as well as the bending moment distribution of the pipe can be obtained.

The spatial configuration and bending moment of the pipe as well as the force of the pipe on the nodule collector were analyzed by changing the nodule collector position and buoyancy material arrangement.

(1) Influence of the nodule collector positions

The flow velocity of the seawater was assumed to be zero. The pipe equilibrium configuration (Fig. 6) and the static force of the pipe on the nodule collector (Fig. 7) were simulated at nodule collector positions of (100, 150, 0), (100, 200, 0), (100, 250, 0), (100, 300, 0), and (100, 350, 0), respectively.

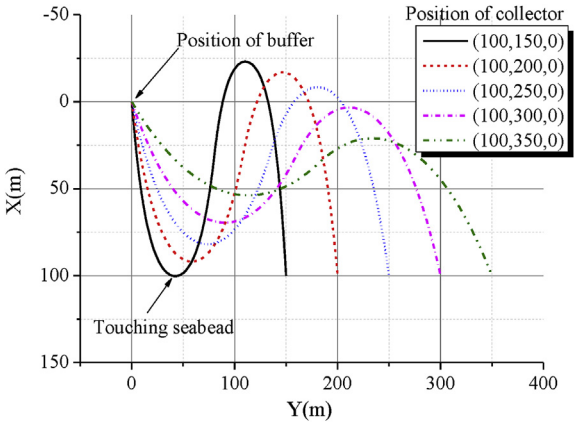

Fig. 6. Equilibrium configuration at different nodule collector positions.

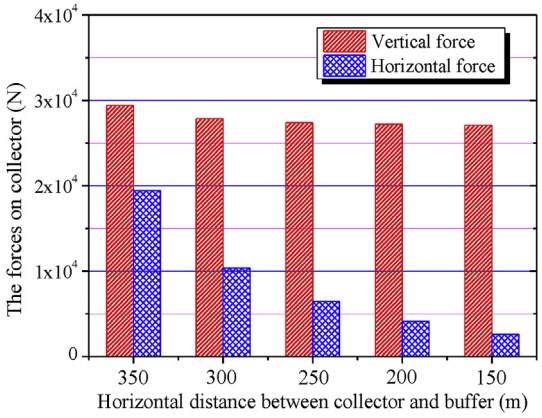

Fig. 7. The force exerted by the pipe on the nodule collector at different nodule collector positions.

The analysis showed that when the horizontal distance between the nodule collector and the buffer was 150 m, the pipe will touch the seabed. This distance value should be the smallest distance between the nodule collector and the buffer. Moreover, the horizontal and vertical forces exerted by the pipe on the nodule collector increased with this distance (Fig. 7). According to the results of the equilibrium configurations and the forces on the nodule collector, the favorable working horizontal distance between the nodule collector and the buffer is in the range of 200 m–300 m.

(2) Effect of buoyancy material

According to the position of the buoyancy material and the magnitude of the buoyancy, six cases are studied, namely:

Case 1. Buoyancy bodies are set within the half-length of the pipe on the collector side, and the buoyancy equals the wet weight of the pipe;

Case 2. Buoyancy bodies are set within the half-length of the pipe on the collector side, and the buoyancy is twice the wet weight of the pipe;

Case 3. Buoyancy bodies are set within the half-length of the pipe on the collector side, and the buoyancy is three times the wet

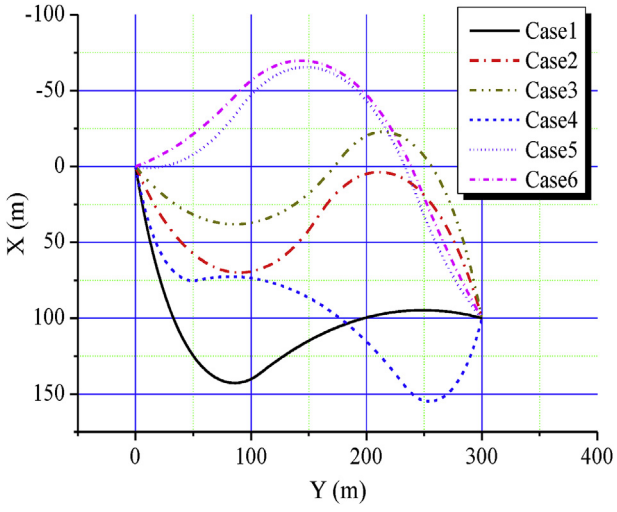

Fig. 8. Equilibrium configurations of the pipe at different buoyancy materials and arrangements.

weight of the pipe;

Case 4. Buoyancy bodies are set within the part between 1/4 and 3/4 of the pipe, and the buoyancy equals the wet weight of the pipe;

Case 5. Buoyancy bodies are set within the part between 1/4 and 3/4 of the pipe, and the buoyancy is twice the wet weight of the pipe;

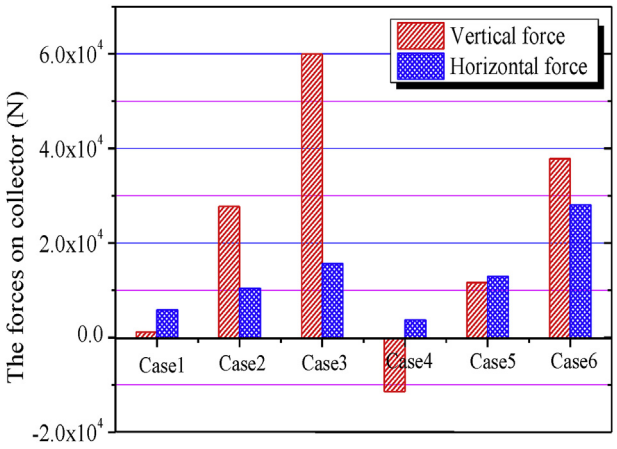

Fig. 9. The force exerted by the pipe on the nodule collector at different buoyancy materials and arrangements.

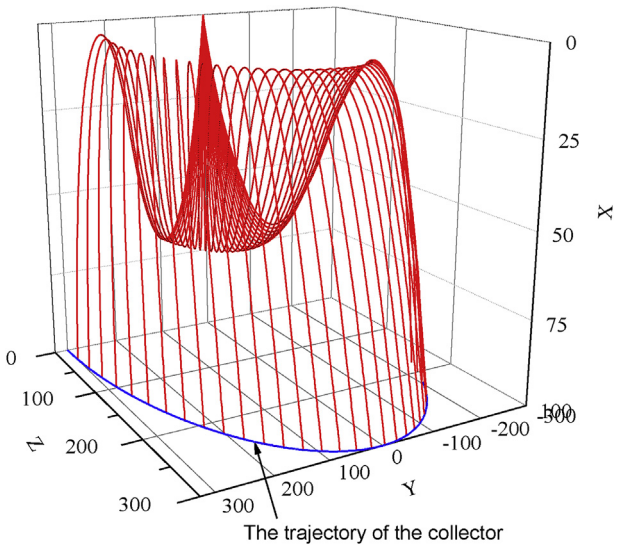

Fig. 10. Spatial configuration of the pipe when the nodule collector travels in a circle.

Case 6. Buoyancy bodies are set within the part between 1/4 and 3/4 of the pipe, and the buoyancy is three times the wet weight of the pipe.

Figs. 8 and 9 show the simulations of the equilibrium configurations and forces acting on the collector in these six cases. When the weight buoyancy material is twice the wet weight (cases 2 and 5), the spatial configuration is more suitable for transportation, and the force acting on the collector in Case 5 is smaller than that in Case 2.

5.2. Dynamic response analysis

In this section, the dynamic analysis of flexible mining pipe was carried out assuming that the nodule collector and buffer are in motion. The static state, in which the position of the nodule collector is (100, 300, 0), was set as the initial state of the dynamic analysis. The following four cases were considered:

1) The buffer does not move, and the collector travels in a circle (i.e., the nodule collector moves in a circle around the buffer on the seabed) at a running speed of 0.5 m/s;
2) The buffer does not move, and the collector makes a roundtrip travel (i.e., the nodule collector moves back and forth within 200 m–300 m from the buffer on the seabed), at a running speed of 0.5 m/s;
3) The collector does not move, and the buffer moves in a simple harmonic heave oscillation with a 5 m amplitude and periods are 10s and 40s, respectively;
4) The collector does not move, and the buffer moves a simple harmonic surge oscillation with a 10 m amplitude and periods are 15s and 60s, respectively.

Figs. 10 and 11 show the 3-D spatial configuration of the pipe and the force acting on the nodule collector when the nodule collector is traveling in a circle. Figs. 12 and 13 show those when the nodule collector is moving in a roundtrip travel. The results indicated that when the collector travels back and forth, the movement pattern of the pipe changes greatly, and its force on the nodule collector changes more drastically and show large fluctuations, especially when the collector changes the direction of the movement. This means that the pipe will undergo large oscillations, which negatively affects the safe operation of the collector and the whole mining system. On the other hand, when the collector travels in a circle on the seabed, the spatial configuration and the force on the collector show gradual changes. Therefore, a circular travel of the collector is more advantageous for safe mining.

Figs. 14 and 15 show the forces on the collector when the buffer is periodically heaving, and Figs. 16 and 17 show the forces on the collector when the buffer is periodically surging. The results show that at high frequency of the heave and surge, the forces of the pipe on the nodule collector experience few high-frequency

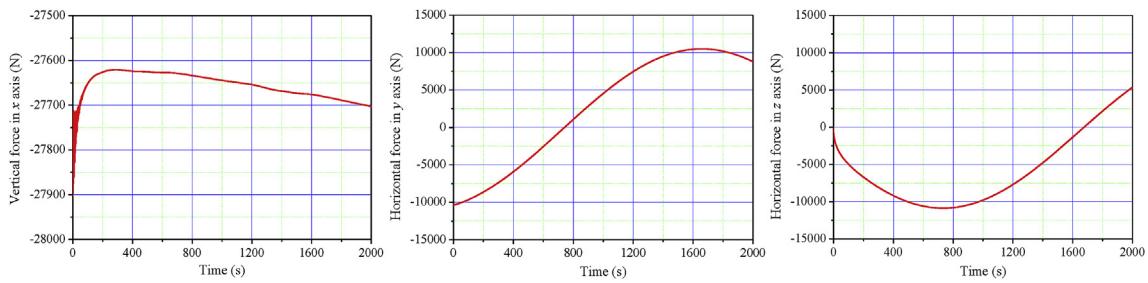

Fig. 11. The force exerted by the pipe on the nodule collector traveling in a circle.

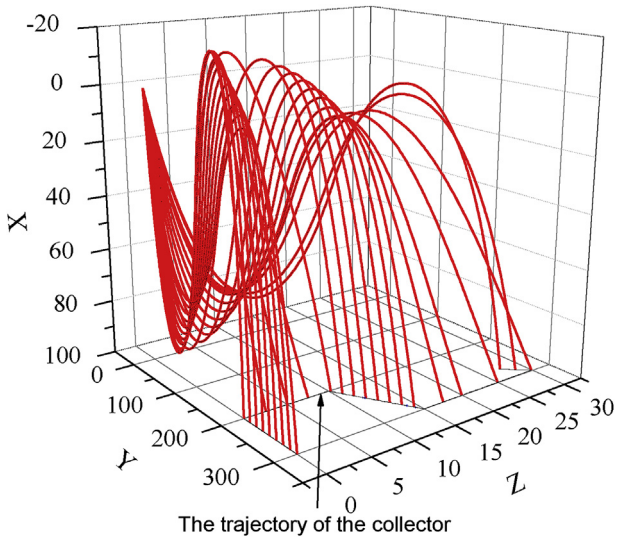

Fig. 12. The spatial configuration of the pipe when the nodule collector moves back and forth within the range of 200 m–300 m.

fluctuations, which gradually increase with time. This phenomenon results in a drastic fluctuation of the forces on the collector and may cause accidents (Figs. 14 and 16). However, when the buffer undergoes a low-frequency oscillation, the force of the pipe on the collector shows drastic fluctuations. The analysis shows that it is necessary to suppress the high-frequency oscillation of the buffer to maintain the safety of the mining system.

The above results are dynamic responses of mining flexible pipe caused by the drastic movement of the collector and buffer, and the displacement of the pipe is much larger than its deformation. The results indicate that the VFIFE method can easily and efficiently solve the geometric nonlinear problem of large displacement and small deformation and obtain the time history of the responses, bending moment, and tension force. These results prove the advantages of the VFIFE method.

6. Conclusions

This study applied the VFIFE method to the static and dynamic response analysis of deep-sea flexible pipes. This study offered a solution to manage the distributed loads in ocean environment using the VFIFE theory. A simulation program was constructed and verified. Next, a simulation example was conducted based on a flexible mining pipe. The VFIFE method was proved to be an easier and more efficient method for the three-dimensional static and dynamic analyses of deep-sea slender members, such as SCR, TTR, and flexible pipes.

The numerical analysis was conducted based on the 1000-m sea trial system in China. It was concluded that: (1) The best horizontal working distance between the collector and the buffer is within the range of 200–300 m. (2) To reduce the influence of flexible pipes on the operation safety of the collector, it should move in a circular motion not in a roundtrip travel. (3) The high-frequency heaving and surging motion of the buffer can cause drastic fluctuations in the force exerted by the flexible pipes on the collector and the buffer, which leads to system damage. Therefore, it is necessary to suppress the high-frequency heaving and surging of the buffer to ensure the mining safety.

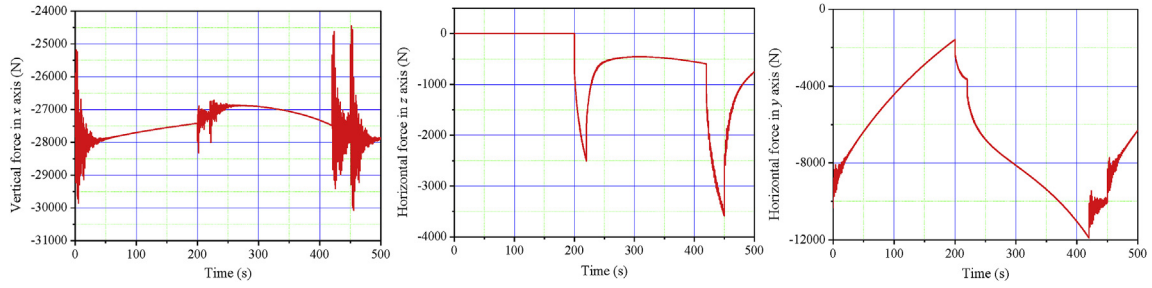

Fig. 13. The force exerted by the pipe on the nodule collector moving back and forth within the range of 200 m–300 m.

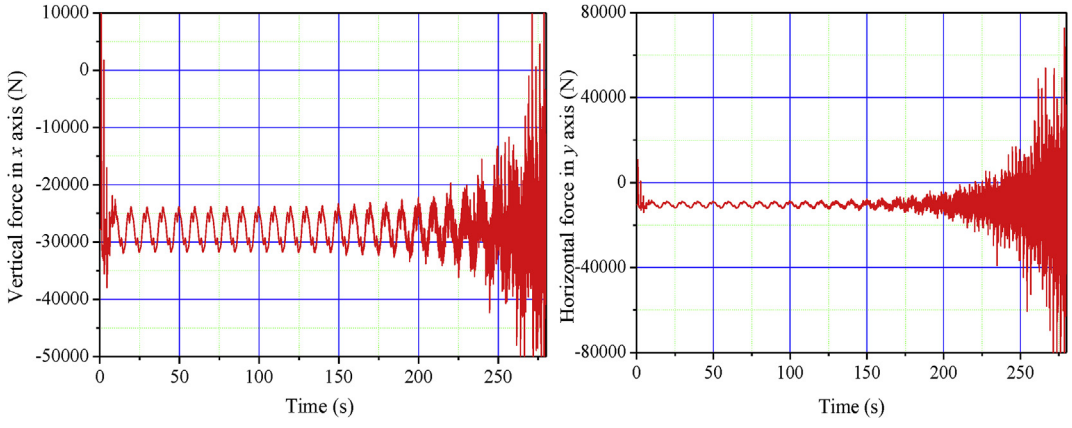

Fig. 14. Forces exerted by the pipe on the nodule collector: (a) vertical force; (b) horizontal force (heave period = 10 s, amplitude = 5 m).

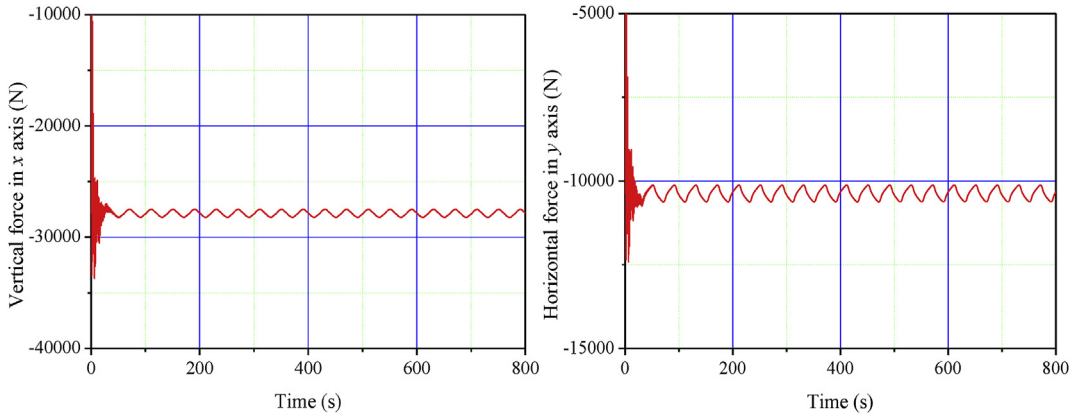

Fig. 15. Forces exerted by the pipe on the nodule collector: (a) vertical force; (b) horizontal force (heave period = 40 s, amplitude = 5 m).

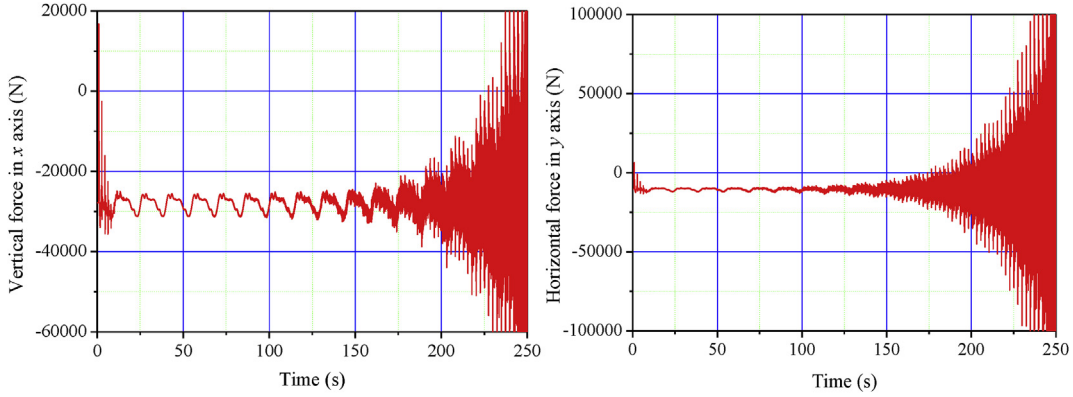

Fig. 16. Forces exerted by the pipe on the nodule collector: (a) vertical force; (b) horizontal force (surge period = 15 s, amplitude = 10 m).

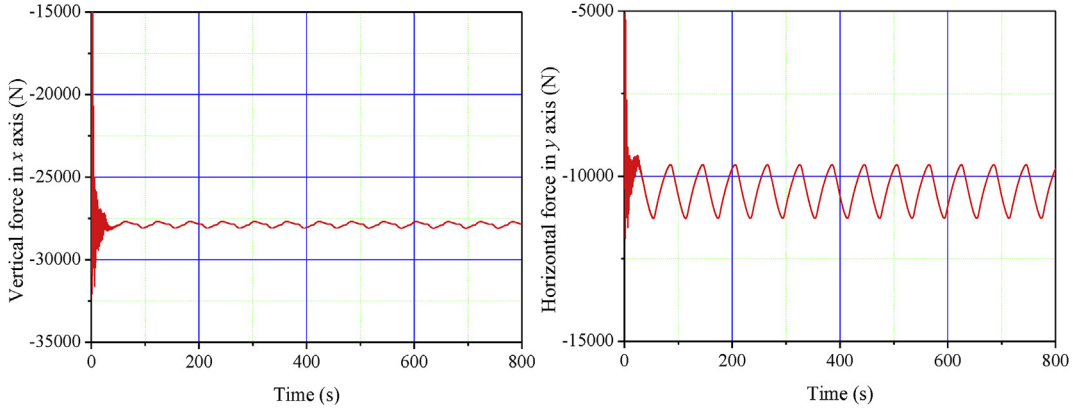

Fig. 17. Forces exerted by the pipe on the nodule collector: (a) vertical force; (b) horizontal force (surge period = 60 s, amplitude = 10 m).

Acknowledgements

This study was supported by the National Natural Science Foundation of China (Grants 51805522, 11672306, and 51490673), State Key Laboratory of Hydraulic Engineering Simulation and Safety (Tianjin University) (Grant HESS1601), the Strategic Priority Research Program of the Chinese Academy of Sciences (Grant XDB22020100), and the Informatization Plan of the Chinese Academy of Sciences (Grant XXH13506-204).

References

Bai, X.L., Huang, W., Vaz, M.A., Yang, C., Duan, M., 2015. Riser-soil interaction model effects on the dynamic behavior of a steel catenary riser. Mar. Struct. 41, 53–76.

Brown, P.A., Soltanahmadi, A., Chandwani, R., 1989. Application of the finite difference technique to the analysis of flexible riser systems. In: Proceedings of the Fourth International Conference on Civil and Structural Engineering Computing, pp. 225–232.

Burgess, J.J., 1991. Modeling of undersea cable installation with a finite difference method. In: Proceedings of First International Offshore and Polar Engineering Conference, pp. 222–227.

Chang, P.Y., Lee, H.H., Tseng, G.W., Chung, P.Y., 2010. VFIFE method applied for offshore template structures upgraded with damper system. J. Mar. Sci. Technol.

18 (4), 473–483.
Chatjigeorgiou, I.K., 2008. A finite differences formulation for the linear and nonlinear dynamics of 2D catenary risers. Ocean Eng. 35, 616–636.
Chatjigeorgiou, I.K., 2010. Three dimensional nonlinear dynamics of submerged, extensible catenary pipes conveying fluid and subjected to end-imposed excitations. Int. J. Non Lin. Mech. 45 (7), 667–680.
Duan, Y.F., He, K., Zhang, H.M., Ting, E.C., Wang, C.Y., Chen, S.K., Wang, R.Z., 2014. Entire-process simulation of earthquake-induced collapse of a mockup cable-stayed bridge by vector form intrinsic finite element (VFIFE) method. Adv. Struct. Eng. 17 (3), 347–360.
Duan, Y.F., Wang, S.M., Yau, J.D., 2019. Vector form intrinsic finite element method for analysis of train-bridge interaction problems considering the coach-coupler effect. Int. J. Struct. Stabil. Dynam. 19 (2), 1950014.
Garrett, D.L., 1982. Dynamic analysis of slender rods. J. Energ. Resour. 104 (4), 302–306.
Ghadimi, R., 1988. A simple and efficient algorithm for the static and dynamic analysis of flexible marine risers. Comput. Struct. 29 (4), 541–555.
Hou, X.Y., Fang, Z.D., 2018. Solid structure analysis with large deformation of eight-node hexahedral element using vector form intrinsic finite element. Adv. Struct. Eng. 21 (6), 852–861.
Hou, X.Y., Fang, Z.D., Zhang, X.J., Universit, N.P., 2018. Static contact analysis of spiral bevel gear based on modified VFIFE (vector form intrinsic finite element) method. Appl. Math. Model. 60, 192–207.
Jain, A.K., 1994. Review of flexible risers and articulated storage systems. Ocean Eng. 21 (8), 733–750.
Lee, H.H., Tseng, K.W., Chang, P.Y., 2007. The Application of vector form intrinsic finite element method to template offshore structures. In: Computational Mechanics. Springer, Berlin.
Li, X.M., Ma, J.F., Guo, H.Y., 2018a. Geometrical configuration and internal force analysis of steel catenary riser. Period. Ocean U. China. 48 (10), 116–122 (in Chinese).
Li, X.M., Zhang, L., Niu, J.J., Han, Y.Q., Guo, H.Y., 2016. Dynamic response of a deep-sea top tensioned riser based on vector form intrinsic finite element. J. Vib. Shock 35 (11), 218–223 (in Chinese).
Li, X.M., Guo, X.L., Guo, H.Y., 2018b. Vector form intrinsic finite element method for the two-dimensional analysis of marine risers with large deformations. J. Ocean Univ. China 17 (3), 498–506.
Lu, Z.G., Yao, J., 2012. Vector form intrinsic finite element - a new numerical method. Spatial Struct. 18 (1), 85–91 (in Chinese).
McNamara, J.F., Hibbit, H.D., 1986. Numerical analysis of flexible pipes and risers in offshore applications. In: Proceedings of the First Offshore and Arctic Frontiers, pp. 343–352.
McNamara, J.F., O'Brien, P.J., Gilroy, S.G., 1988. Nonlinear analysis of flexible risers using hybrid finite elements. J. Offshore. Mech. Arct. 110 (3), 197–204.
Owen, D.G., Qin, K., 1986. Model tests and analysis of flexible riser systems. In: Proceedings of the Fifth International Symposium on Offshore Mechanics and Arctic Engineering, pp. 133–145.
Park, H.I., Jung, D.H., 2002. A finite element method for dynamic analysis of long slender marine structures under combined parametric and forcing excitations. Ocean Eng. 29 (11), 1313–1325.
Patel, M.H., Seyed, F.B., 1995. Review of flexible riser modelling and analysis techniques. Eng. Struct. 17 (4), 293–304.
Raman-Nair, W., Baddour, R.E., 2003. Three-dimensional dynamics of a flexible marine riser undergoing large elastic deformations. Multibody Syst. Dyn. 10 (3), 393–423.
Sakamoto, T., Hobbs, R.E., 1995. Nonlinear static and dynamic analysis of three-dimensional flexible risers. In: The Fifth International Offshore and Polar Engineering Conference, 11-16 June, Hague, Netherlands.
Shih, C., Wang, Y.K., Ting, E.C., 2004. Fundamentals of a vector form intrinsic finite element: Part III. Convected material frame and examples. J. Mech. 20 (2), 133–143.
Ting, E.C., Shih, C., Wang, Y.K., 2004a. Fundamentals of a vector form intrinsic finite element: Part I. Basic procedure and a plane frame element. J. Mech. 20 (2), 113–122.
Ting, E.C., Shih, C., Wang, Y.K., 2004b. Fundamentals of a vector form intrinsic finite element: Part II. Plane solid elements. J. Mech. 20 (2), 123–132.
Ting, E.C., Duan, Y.F., Wu, T.Y., 2012. Vector Mechanics of Structures. Science Press, Beijing (in Chinese).
Webster, W.C., Kim, J., Lambrakos, K., Jing, X.N., 2012. Rod dynamics with large stretch. Proceedings of the ASME 2012 31-st International Conference on Ocean. Offshore and Arctic Engineering, p. 83889.
Wu, T.Y., 2013. Dynamic nonlinear analysis of shell structures using a vector form intrinsic finite element. Eng. Struct. 56, 2028–2040.
Wu, T.Y., Wang, C.Y., Chuang, C.C., Ting, E.C., 2007. Motion analysis of 3D membrane structures by a vector form intrinsic finite element. J. Chin. Inst. Eng. 30 (6), 961–976.
Xiao, F.Q., 2012. The Spatial Configuration Analysis and the Fluid-Structure Coupling Mechanics of the Hose in Deep-Ocean Mining System. Central South University.
Xu, L.G., Lin, M., 2017. Analysis of buried pipelines subjected to reverse fault motion using the vector form intrinsic finite element method. Soil Dynam. Earthq. Eng. 93, 61–83.